RSC Advances

ROYAL SOCIETY OF CHEMISTRY

www.rsc.org/advances

Cite this: DOI: 10.1039/c0xx00000x

www.rsc.org/xxxxxx

ARTICLE TYPE

Highly active Au–Pd nanoparticles supported on three-dimensional graphene–carbon nanotube hybrid for selective oxidation of methanol to methyl formate†

Ruiyi Wang,[ab] Zhiwei Wu,[a] Guofu Wang,[a] Zhangfeng Qin,*[a] Chenmeng Chen,[c] Mei Dong,[a] Huaqing Zhu,[a] Weibin Fan[a] and Jianguo Wang*[a]

Received (in XXX, XXX) Xth XXXXXXXXX 20XX, Accepted Xth XXXXXXXXX 20XX
DOI: 10.1039/b000000x

Au–Pd nanoparticles supported on graphene–carbon nanotube hybrid exhibit high catalytic activity in selective oxidation of methanol to methyl formate at low temperature, owning to the strong interaction between graphene and Au–Pd as well as the spacing and bridging effect of nanotube inserter on the hybrid three-dimensional structure.

Selective oxidation of alcohols to corresponding carbonyl compounds such as ketones, aldehydes and esters is a viable approach to get various valuable chemicals.[1–5] However, such a process often involves the use of stoichiometric oxygen donors such as dichromate, permanganate and hydrogen peroxide, which are either costly or harmful to the production facilities and environment.[6,7] As a result, a great deal of effort has been made to explore the catalytic oxidation processes with molecular oxygen as an oxidant; among them, the selective oxidation of methanol to methyl formate (MF) is regarded as an environmentally benign route to get valuable methanol-down-stream products. Wide array of catalysts have been reported in methanol oxidation, including non-noble metal oxides (SnO_2-Mo_2O_3, V_2O_5-TiO_2 and Fe_2O_3/SiO_2),[8–12] heteropoly acids[13] and supported noble metals[14]; however, their performances (in terms of methanol conversion and selectivity to MF at low temperature) are still somewhat insufficient for practical application.

Ever since the excellent work of Wittstock and coworkers on the synthesis of MF over AuAg alloy catalyst at low temperature,[15] alcohol oxidation over bimetallic catalysts under mild conditions has attracted extensive attentions.[16–18] In our previous work, Au–Pd bimetallic nanoparticles supported on graphene (Au–Pd/Graphene) exhibit high catalytic activity in the selective oxidation of methanol to MF, owing to the synergism of Au and Pd as well as the strong interaction between graphene and Au–Pd nanoparticles.[18]

Graphene, a single layer of carbon atoms densely packed into a hexagonal honeycomb network, is a promising catalyst support owing to its large surface area, special structure and unique conductive properties. A series of graphene-supported monometallic and bimetallic nanoparticles such as Pt[19,20], Pd[21,22], Au[23], Pd–Ag[24] and Au–Pd[25] exhibited impressive catalytic performance in various reactions. However, graphene as a catalyst support is prone to agglomerate irreversibly in the moulding process due to the strong π–π stacking and van der Waals interaction,[26] which is deleterious to the catalytic activity. To solve this problem, Si and Samulski used platinum nanoparticles of 3–4 nm in diameter as a spacing inserter adhered to graphene;[27] however, it is difficult to get stable metallic nanoparticles with an appropriate size to inhibit the face to face aggregation of graphene sheets. Recently, doping with carbon nanotubes (CNT) have been widely used to modify the graphene sheets, especially in the field of electrochemistry.[28–32] The incorporation of CNT can effectively inhibit the irreversible aggregation of graphene and even bridge the defects of graphene sheets and improve its electrons transfer capacity.[21,33]

To enhance the catalytic activity of Au–Pd/Graphene, in this work, graphene (Gr) was doped with carbon nanotubes (CNT). The Gr–CNT hybrids were obtained by the solution self-assemble method (ESI†), i.e. by sonicating the aqueous colloidal suspensions of graphene oxide (GO) and acid functionalized CNT (Fig. S1, ESI†); the Gr–CNT hybrids are denoted as Gr–CNT(*w*), where *w* is the weight ratio of graphene to carbon nanotubes. With Gr–CNT(*w*) as the support, Au–Pd/Gr–CNT(*w*) catalysts were prepared through the deposition–precipitation method (ESI†),[18] where the loadings of Au and Pd were designed to be 2 and 1 wt.%, respectively. The actual loadings of Au and Pd were also determined by inductively coupled plasma atomic emission spectroscopy (ICP-AES), as given in Table S1, ESI†, which proves that the actual loadings of Au and Pd are very close to the designed values and the loss of Au and Pd is negligible upon the aqueous rinsing during the catalyst preparation.

The textural properties of carbon nanotubes (CNT), graphene (Gr), Gr–CNT hybrids, and corresponding supported Au–Pd catalysts were measured by nitrogen physisorption, as given in Table 1. Although graphene sheets may have a theoretical surface area of 2600 $m^2\ g^{-1}$, the surface area of graphene used in this work is only about 218.8 $m^2\ g^{-1}$, due to the face to face aggregation of graphene sheets. After doping graphene with CNT (186.4 $m^2\ g^{-1}$), the resultant Gr–CNT(5) hybrid displays a surface area of 311.6 $m^2\ g^{-1}$, which is much higher than that of either graphene or CNT, suggesting tha

the aggregation of graphene sheets is effectively inhibited by the incorporation of CNT as a spacing inserter. A series of Gr–CNT(*w*) hybrids with different Gr/CNT mass ratios all display a sorption isotherm of type IV with a hysteresis loop according to the IUPAC classification, meaning that they have a mesoporous structure (Fig. S3, ESI†); moreover, a Gr/CNT mass ratio of 5 gives the best doping effect, viz., the highest surface area and mesopore volume. Table 1 also illustrates that after the loading of Au–Pd nanoparticles, the surface areas of Au–Pd catalysts are only slightly decreased, in comparison with the corresponding supports, suggesting that the deposition-precipitation process has little influence on the structure of carbonaceous supports.

Table 1 Textural properties of the graphene–carbon nanotube (Gr–CNT) hybrids and Au–Pd/Gr–CNT catalysts and their catalytic performance in methanol oxidation [a]

Sample	Surface area (m^2 g^{-1})	Pore volume (cm^3 g^{-1})	Pore size (nm)	Particle size [b] (nm)	x_{MeOH} [c] (%)	s_{MF} [c] (%)	TOF [d] (h^{-1})
CNT	186.4	0.574	12.3	--	--	--	--
Gr	218.8	0.501	9.2	--	--	--	--
Gr–CNT(5)	311.6	0.824	10.6	--	--	--	--
Au–Pd/CNT	175.3	0.584	13.3	20.5	0.6	100	2.1
Au–Pd/Graphene	193.7	0.562	11.6	7.5	35.3	100	132
Au–Pd/Gr–CNT(5)	301.4	0.724	10.5	3.3	42.5	100	150

[a] The reactions were carried out at 45 °C (ESI†); 60 mg catalyst was loaded and the feed stream consisted of 6.4 vol.% CH_3OH, 70.2 vol.% O_2, and balanced argon, with a flow rate of 42.8 mL min^{-1}, equivalent to a gas hourly space velocity (GHSV) of 42,800 mL g^{-1} h^{-1}; the loadings of Au and Pd for all supported Au–Pd catalysts are 2 and 1 wt.%, respectively. [b] Mean particle sizes were estimated by measuring the sizes of randomly selected 100 typical particles in the TEM images. [c] The products consist of MF and CO_2. The conversion of methanol x_{MeOH} is determined by $x_{MeOH} = (n_{MeOH,feed} - n_{MeOH,outlet})/n_{MeOH,feed} \times 100\%$ and the selectivity to each product (s_i) is determined by $s_i = (n_{i,outlet} \times k_i)/(n_{MeOH,feed} - n_{MeOH,outlet}) \times 100\%$, where k_i is the carbon number in one molecule of product i (ESI†). [d] Turnover frequency (TOF), the number of methanol molecules converted to MF per active site and hour, is estimated on basis of total Au and Pd atoms at 45 °C (ESI†).

As shown in Fig. 1, an intense peak at 12.22°, typical for C(001), is present in the X-ray diffraction (XRD) pattern of graphene oxide (GO). After reduction, a new diffraction peak at 25.51° corresponding to C(002) appears at the XRD pattern of graphene, in which most of the oxygen-containing functional groups are removed. Compared with graphene, the characteristic C(002) peaks of Gr–CNT(5), Gr–CNT(3) and Gr–CNT(1) hybrids are shifted slightly to higher angles due to the incorporation of CNT. After the loading of Au–Pd particles, the characteristic peaks at 38.19° and 44.38°, corresponding to Au(111) and Au(200), respectively, are observed in the XRD pattern of Au–Pd/Gr–CNT(5), whereas no diffraction peaks for Pd are detected, probably due to its relatively low content and high dispersion.

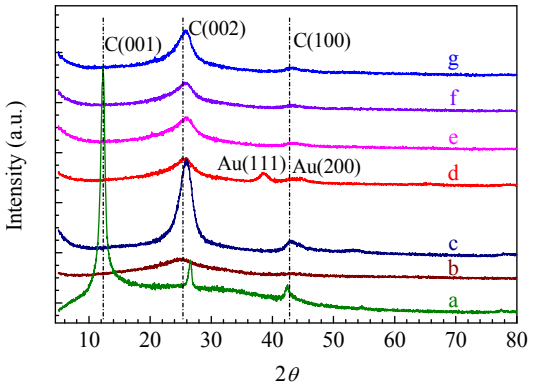

Fig. 1 XRD patterns of (a) graphene oxide (GO), (b) graphene (Gr), (c) carbon nanotubes (CNT), (d) Au–Pd/Gr–CNT(5), (e) Gr–CNT(5), (g) Gr–CNT(3), and (h) Gr–CNT(1).

For Au–Pd/Gr–CNT(5), the scanning electron microscope (SEM) image in Fig. 2a shows that carbon nanotubes are uniformly inserted into the two layers of graphene sheets, suggesting that three dimension (3D) Gr–CNT hybrids are formed by the solution self-assemble method (ESI†). The transmission electron microscope (TEM) image in Fig. 2b indicates that spherical Au–Pd nanoparticles are uniformly dispersed on the surface of Gr–CNT hybrids. The HRTEM image in Fig. 2c illustrates that the particles of Au–Pd alloy with a d-spacing of 0.230 nm are mainly anchored on the interfaces of carbon nanotubes and graphene nanosheets; it is estimated by randomly selecting 100 typical particles that the particle size of Au–Pd alloy is in the range of 1–8 nm with an average of 3.3 nm (Fig. 2d). Comparatively, the Au–Pd particles in Au–Pd/Graphene and Au–Pd/CNT have a mean particle size of 7.5 and 20.5 nm, respectively. The doping of graphene with CNT is propitious to reduce the size of metal particles dispersed on the hybrid support, owing to the high surface area and confined space of the Gr–CNT hybrids. Moreover, as the Au–Pd particle size in Au–Pd/Gr–CNT(5) is greatly reduced, the Au–Pd alloying degree in Au–Pd/Gr–CNT(5) is also enhanced markedly, in comparison with the partial alloying of twined Au–Pd structure in Au–Pd/Graphene.[18] Wang and coworkers also found that gold nanoparticles aggregation can be effectively inhibited when entrapped or confined by the "rigid" mesoporous carbonaceous framework.[31]

The X-ray photoelectron spectroscopy (XPS) spectra of Au–Pd supported on CNT, graphene and Gr–CNT(5) are shown in Fig. 3. Au 4*f* spectra can be fitted into four peaks (Fig. 3I), two peaks for Au^0 centered at binding energies (BEs) of 84.0 and 87.6 eV and other two for cationic gold species $Au^{\delta+}$ centered at 85.3 and 89.2 eV.[34] In Pd 3*d* XPS spectra, the peaks at 335.6 and 340.8 eV are attributed to Pd^0 species and the peaks around 338.1 and 343.9 eV are related to Pd^{2+} species (Fig. 3II). In comparison with those of Au–Pd/CNT and Au–Pd/Graphene, the peaks for both Au^0 and Pd^0 in the XPS spectra of Au–Pd/Gr–CNT(5) are shifted distinctly towards lower BEs, suggesting that the synergism of Au–Pd bimetallic nanoparticles is enhanced in Au–Pd/Gr–CNT(5). Venezia and coworkers also observed evident shifts of both

Au $4f_{7/2}$ and Pd 3*d* spectra towards lower BEs for bimetallic gold-palladium catalysts, compared with monometallic gold and palladium catalysts, indicating an electronic interaction between gold and palladium.[35]

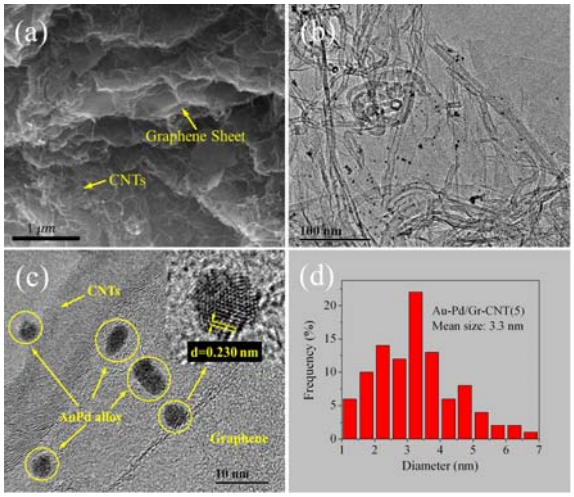

Fig. 2 SEM image (a), TEM image (b), HRTEM image (c), and Au–Pd particle size distribution (d) of the Au–Pd/Gr–CNT(5) catalyst.

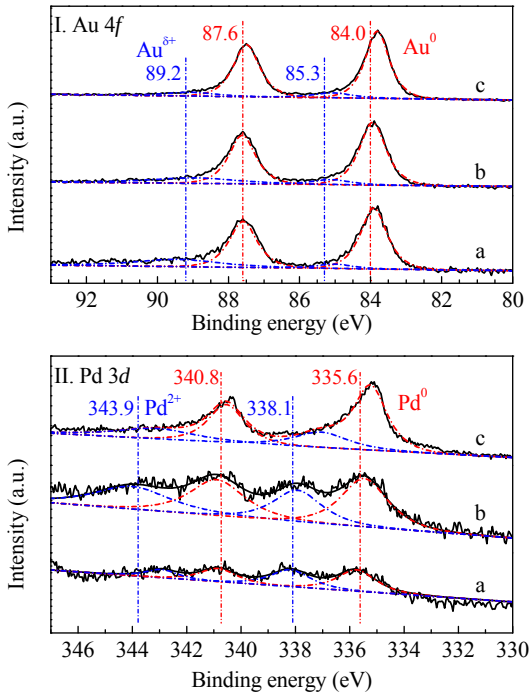

Fig. 3 Au 4*f* (I) and Pd 3*d* (II) XPS spectra of (a) Au–Pd/CNT, (b) Au–Pd/Graphene and (c) Au–Pd/Gr–CNT(5) catalysts.

It was considered that CNT inserted between graphene nanosheets may act as a bridge connecting the defects for electron transfer and then improve their conductivity and catalytic activity.[21,33] Moreover, the graphene support is rich in π electrons, which can promote the reduction of Pd^{2+} to Pd^0 with the help of Au atoms in AuPd alloy.[18] In this work, the XPS results further illustrate that the electron exchange between gold and palladium is greatly enhanced in Au–Pd/Gr–CNT(5) by doping graphene with CNT; the fraction of Pd^0 in Au–Pd/Gr–CNT(5) is about 67.3%, much higher than the value of 56.7% in Au–Pd/Graphene (Table S2, ESI†).

The states of Pd on various carbonaceous supports are further determined by the X-ray absorption near-edge spectroscopy (XANES), as shown in Fig. 4. In the Pd K-edge XANES spectra, the absorption threshold resonance, called a white line, appears between 24 360 and 24 380 eV, corresponding to the electronic transitions that arise from 1s to unoccupied 4p states above the Fermi level. The second (24 385 eV) and third (24 435 eV) peaks are attributed to 1s to dp and 1s to dsp transitions, respectively. The white line intensity is sensitive to the change in electron occupancy of valance orbital and can be used to estimate the density of unoccupied states and the change in the state of Pd species, whereas the energy shift is related to a change in the effective number of valence electrons at the absorbing site. Fig. 4 shows that Pd/Graphene is similar to PdO reference in the edge, suggesting that Pd^{2+} is the major Pd species in Pd/Graphene. For Au–Pd/Graphene, however, a fraction of Pd^{2+} is reduced to Pd^0; after doping graphene with CNT, the fraction of Pd^{2+} reduced to Pd^0 in Au–Pd/Gr–CNT(5) is even higher. A quantitative analysis with PdO and Pd foil as references (Table S2, ESI†) illustrates that the fractions of Pd^0 in Au–Pd/Gr–CNT(5) and Au–Pd/Graphene are about 75.0% and 61.3%, respectively.

It was considered that both Pd^0 and Pd^{2+} may be involved in the catalytic reaction cycles for methanol oxidation; however, CNT inserted in graphene sheets may greatly improve the redox properties of the resultant Au–Pd/Gr–CNT(5) catalyst and then enhance its catalytic activity in methanol oxidation at low temperature. The binding energy shift and the fraction of Pd^0 determined by XPS and XAFS is then a reflection of the extent for the synergy between Au and Pd and the redox ability of these supported Au–Pd catalysts, which is related to their catalytic performance. Therefore, both the XPS and XANES results support that the addition of CNT can improve the conductivity of graphene suppor promote the reduction of PdO and formation of AuPd alloy, and eventually enhance the catalytic activity of Au–Pd supported on the Gr–CNT hybrids.

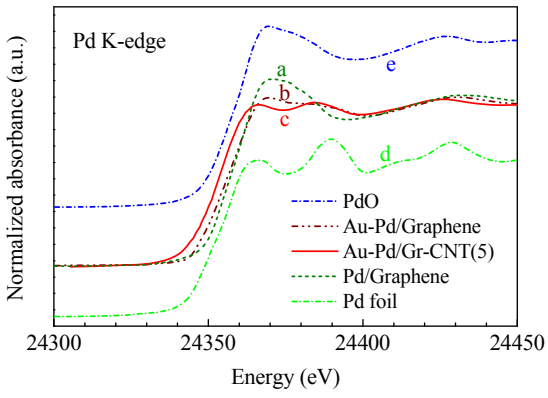

Fig. 4 Pd K-edge XANES spectra of the Pd/Graphene (a), Au–Pd/Graphene (b) and Au–Pd/Gr–CNT(5) (c), with Pd foil (d) and PdO (e) as the references.

The catalytic performance of various catalysts in methanol oxidation was tested in a quartz fixed-bed microreactor (Fig.

S2, ESI†). A series of preliminary characterizations and catalytic tests suggest that a Gr/CNT mass ratio of 5 gives the Au–Pd/Gr–CNT catalysts the best doping effect and the highest activity in methanol oxidation (Figs. S3–S6, ESI†). The conversion of methanol and selectivity to MF along with temperature for methanol oxidation over the Au–Pd/Gr–CNT(5), Au–Pd/Graphene and Au–Pd/CNT catalysts are illustrated in Fig. 5. Au–Pd/CNT is inactive until 50 °C, whereas Au–Pd/Graphene and especially Au–Pd/Gr–CNT(5) exhibit excellent activity at low temperature. At 35 °C, Au–Pd/Graphene gives a methanol conversion of 8.2% and selectivity of 100% to MF, whereas the methanol conversion over Au–Pd/Gr–CNT(5) reaches 15.6%. Table 1 also displays that Au–Pd/Gr–CNT(5) gives a much higher turnover frequency (TOF) than Au–Pd/Graphene and Au–Pd/CNT at low temperature. All these indicate that the doping of graphene with CNT can effectively enhance the activity of Au–Pd bimetallic catalysts in methanol oxidation, especially at low temperature.

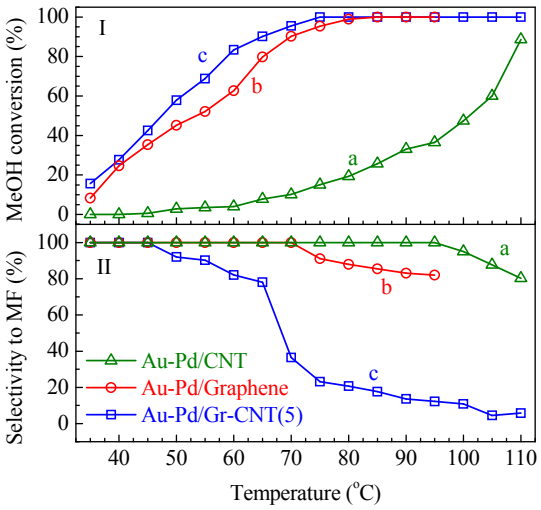

Fig. 5 Conversion of methanol (I) and selectivity to MF (II) along with the reaction temperature for methanol oxidation over (a) Au–Pd/CNT, (b) Au–Pd/Graphene, and (c) Au–Pd/Gr–CNT(5). The loadings of Au and Pd for all supported Au–Pd catalysts are 2 and 1 wt.%, respectively; the feed stream consists of 6.4 vol.% CH_3OH, 70.2 vol.% O_2, and balanced argon, with a gas hourly space velocity (GHSV) of 42,800 mL g^{-1} h^{-1}.

As the pure supports (CNT, Graphene, Gr–CNT) are inert for the methanol oxidation, the catalytic performance of Au–Pd/Graphene + CNT (a physical mixture of Au–Pd/Graphene and CNT) is almost identical to that of Au–Pd/Graphene, as shown in Fig. S7, ESI†, both are much poorer than Au–Pd/Gr–CNT(5). This suggests that it is impossible to insert CNT effectively into the graphene layers through later mechanical mixing. The promoting effect of CNT on the Au–Pd/Gr–CNT(5) catalyst may only appear when the Au–Pd species are supported on the 3D Gr–CNT hybrid, where CNTs are uniformly inserted into the graphene layers through the solution self-assemble method (Fig. 2).

The catalytic activity of Au–Pd/Gr–CNT(5) is also compared with those of some similar catalysts recently reported for methanol oxidation to MF in the literature,[15,36–38] as given in Table S3, ESI†. Although there are many factors that may influence the catalytic performance of a supported catalyst, the nature of support plays an important role in determining the catalyst activity. Au–Pd/Gr–CNT(5), i.e. Au–Pd supported on 3D Gr–CNT hybrid, exhibits higher activity in the selective oxidation of methanol to MF at low temperature, in comparison with those similar catalysts reported recently. The excellent activity of the Au–Pd/Gr–CNT(5) catalyst may be ascribed to the enhanced interaction between graphene and Au–Pd as well as the spacing and bridging effect of the CNT inserter on the hybrid three-dimensional structure.

In conclusion, the incorporation of CNT as a spacing inserter into graphene is effective to inhibit the face to face aggregation of graphene sheets, bridge the defects for electron transfer and stabilize the hybrid three-dimensional structure. As a result, the dispersion of Au–Pd bimetallic particles, the synergy between Au and Pd and the strong interaction between Au–Pd particles and graphene support are enhanced greatly, which endue the Au–Pd bimetallic particles supported on Gr–CNT hybrids with high catalytic activity in methanol oxidation at low temperature. Moreover, such an approach may also be effective to get highly active catalysts with graphene as support for other applications.

The authors thank Dr. J. Ma, Dr. S. Zhang and Prof. Y. Huang at Shanghai Synchrotron Radiation Facility for the help with XAFS measurements as well as the financial support of National Basic Research Program of China (2011CB201400) and National Natural Science Foundation of China (21403268, 21227002, 51302282, 21203231).

Notes and references

[a] *State Key Laboratory of Coal Conversion, Institute of Coal Chemistry, Chinese Academy of Sciences, P.O. Box 165, Taiyuan, Shanxi 030001, PR China. E-mail: qzhf@sxicc.ac.cn (Z. Qin); iccjgw@sxicc.ac.cn (J. Wang)*
[b] *University of Chinese Academy of Sciences, Beijing 100049, PR China*
[c] *Key Laboratory of Carbon Materials, Institute of Coal Chemistry, Chinese Academy of Sciences, P.O. Box 165, Taiyuan, Shanxi 030001, PR China*

† Electronic Supplementary Information (ESI) available: More experimental details and results of catalyst characterization and reaction tests. See DOI: 10.1039/b000000x/

1 D. Enache, J. Edwards, P. Landon, B. Solsona-Espriu, A. Carley, A. Herzing, M. Watanabe, C. Kiely, D. Knight and G. Hutchings, *Science*, 2006, **311**, 362–365.
2 P. Zhang, Y. Gong, H. Li, Z. Chen and Y. Wang, *Nat. Commun.*, 2013, **4**, 1593.
3 R. Jagadeesh, H. Junge, M. Pohl, J. Radnik, A. Brückner and M. Beller, *J. Am. Chem. Soc.*, 2013, **135**, 10776–10782.
4 V. Choudhary, A. Dhar, P. Jana, R. Jha and B. Uphade, *Green Chem.*, 2005, **7**, 768–770.
5 H. Miyamura, T. Yasukawa and S. Kobayashi, *Green Chem.*, 2010, **12**, 776–778.
6 G. Behera and K. Parida, *Appl. Catal. A*, 2012, **413–414**, 245–253.
7 J. Muzart, *Chem. Rev.*, 1992, **92**, 113–140.
8 M. Ai, *J. Catal.*, 1982, **77**, 279–288.
9 G. Liu, Q. Zhang, Y. Han, N. Tsubaki and Y. Tan, *Green Chem.*, 2013, **15**, 1501–1504.
10 Q. Zhang, Y. Tan, G. Liu, J. Zhang and Y. Han, *Green Chem.*, 2014, **16**, 4708–4715.
11 A. Elmi, E. Tronconi, C. Cristiani, J. Martin, P. Forzatti and G. Busca, *Ind. Eng. Chem. Res.*, 1989, **28**, 387–393.
12 C. Wang and R. Willey, *J. Catal.*, 2001, **202**, 211–219.

13 H. Liu and E. Iglesia, *J. Catal.*, 2004, **223**, 161–169.
14 Q. Zhang, Y. Li, L. Zhang, L. Chen, Y. Liu and Y. Lu, *Green Chem.*, 2014, **16**, 2992–2996.
15 A. Wittstock, V. Zielasek, J. Biener, C. M. Friend and M. Baumer, *Science*, 2010, **327**, 319-322.
16 A. Henning, J. Watt, P. Miedziak, S. Cheong, M. Santonastaso, M. Song, Y. Takeda, A. I. Kirkland, S. Taylor and R. Tilley, *Angew. Chem.*, 2013, **125**, 1517–1520.
17 S. Xie, H. Tsunoyama, W. Kurashige, Y. Negishi and T. Tsukuda, *ACS Catal.*, 2012, **2**, 1519–1523.
18 R. Wang, Z. Wu, C. Chen, Z. Qin, H. Zhu, G. Wang, H. Wang, C. Wu, W. Dong, W. Fan and J. Wang, *Chem. Commun.*, 2013, **49**, 8250–8252.
19 P. Kundu, C. Nethravathi, P. Deshpande, M. Rajamathi, G. Madras and N. Ravishankar, *Chem. Mater.*, 2011, **23**, 2772–2780.
20 E. Yoo, T. Okata, T. Akita, M. Kohyama, J. Nakamura and I. Honma, *Nano Lett.*, 2009, **9**, 2255–2259.
21 G. Wu, X. Wang, N. Guan and L. Li, *Appl. Catal. B.*, 2013, **136–137**, 177–185.
22 J. Xu, R. Meng, J. Cao, X. Gu, W. Song, Z. Qi, W. Wang and Z. Chen, *J. Alloys Compounds*, 2013, **564**, 84–90.
23 R. Muszynski, B. Seger and P. Kamat, *J. Phys. Chem. C*, 2008, **112**, 5263–5266.
24 M. Liu, Y. Lu and W. Chen, *Adv. Function. Mater.*, 2013, **23**, 1289–1296.
25 J. Qi, W. Lv, G. Zhang, Y. Li, G. Zhang, F. Zhang and X. Fan, *Nanoscale*, 2013, **5**, 6275–6279.
26 D. Lu, Y. Zhang, S. Lin, L. Wang and C. Wang, *Talanta*, 2013, **112**, 111–116.
27 Y. Si and E. Samulski, *Chem. Mater.*, 2008, **20**, 6792–6797.
28 Z. Zheng, Y. Du, Z. Wang, Q. Feng and C. Wang, *Analyst*, 2013, **138**, 693-701.
29 M. Seol, D. Youn, J. Kim, J. Jang, M. Choi, J. Lee and K. Yong, *Adv. Energy Mater.*, 2014, **4**, 1300775.
30 S. Li, D. Wu, H. Liang, J. Wang, X. Zhuang, Y. Mai, Y. Su and X. Feng, *ChemSusChem*, 2014, **7**, 3002–3006.
31 S. Wang, Q. Zhao, H. Wei, J. Wang, M. Cho, H. Cho, O. Terasaki and Y. Wan, *J. Am. Chem. Soc.*, 2013, **135**, 11849–11860.
32 D. Higgins, M. Hoque, F. Hassan, J. Choi, B. Kim and Z. Chen, *ACS Catal.*, 2014, **4**, 2734–2740.
33 R. Lv, T. Cui, M. Jun, Q. Zhang, A. Cao, D. Su, Z. Zhang, S. Yoon, J. Miyawaki, I. Mochida and F. Kang, *Adv. Function. Mater.*, 2011, **21**, 999–1006.
34 D. Bulushev, I. Yuranov, E. Suvorova, P. Buffat and L. Kiwi-Minsker, *J. Catal.*, 2004, **224**, 8–17.
35 Y. Wang, H. Liu, L. Wang, H. Wang, X. Du, F. Wang, T. Qi, J. Lee and X. Wang, *J. Mater. Chem. A*, 2013, **1**, 6839–6848.
36 L. Merte, M. Ahmadi, F. Behafarid, L. Ono, E. Lira, J. Matos, L. Li, J. Yang and B. Cuenya, *ACS Catal.*, 2013, **3**, 1460–1468.
37 G. Whiting, S. Kondrat, C. Hammond, N. Dimitratos, Q. He, D. Morgan, N. Dummer, J. Bartley, C. Kiely, S. Taylor and G. Hutchings, *ACS Catal.*, 2014, **4**, 637–644.
38 R. Wojcieszak, M. Ghazzal, E. Gaigneaux and P. Ruiz, *Catal. Sci. Technol.*, 2014, **4**, 738–745